Research Article | Vol. 30, No. 26 / 19 Dec 2022 / Optics Express 47867

Optics EXPRESS

Broadband soft X-ray source from a clustered gas target dedicated to high-resolution XCT and X-ray absorption spectroscopy

KAROL A. JANULEWICZ,[1] ŁUKASZ WĘGRZYŃSKI,[1] TOMASZ FOK,[1] ANDRZEJ BARTNIK,[1] HENRYK FIEDOROWICZ,[1] SŁAWOMIR SKRUSZEWICZ,[2] MARTIN WÜNSCHE,[3,4] ERICH ECKNER,[3,4] SILVIO FUCHS,[3,4,5] JULIUS REINHARD,[3,4] JOHANN J. ABEL,[3] FELIX WIESNER,[3,4] GERHARD. G. PAULUS,[3,4] CHRISTIAN RÖDEL,[6] CHUL MIN KIM,[7] AND PRZEMYSŁAW W. WACHULAK[1,*]

[1] *Institute of Optoelectronics, Military University of Technology, 00-908 Warsaw, Poland*
[2] *Deutsches Elektronen-Synchrotron DESY, Noltkestr. 85, 22607 Hamburg, Germany*
[3] *Institute of Optics and Quantum Electronics, Friedrich Schiller University Jena, Max-Wien-Platz 1, 07743 Jena, Germany*
[4] *Helmholtz Institute Jena, Fröbelstieg 3, 07743 Jena, Germany*
[5] *Laserinstitut Hochschule Mittweida, Technikumplatz 17, 09648 Mittweida, Germany*
[6] *Institute of Nuclear Physics, TU Darmstadt, Schlossgartenstraße 9, 64289 Darmstadt, Germany*
[7] *Advanced Photonics Research Institute, Gwangju Institute of Science and Technology, 61005 Gwangju, Republic of Korea*
[*] *wachulak@gmail.com*

Abstract: The development of the broad-bandwidth photon sources emitting in the soft X-ray range has attracted great attention for a long time due to the possible applications in high-resolution spectroscopy, nano-metrology, and material sciences. A high photon flux accompanied by a broad, smooth spectrum is favored for the applications such as near-edge X-ray absorption fine structure (NEXAFS), extended X-ray absorption fine structure (EXAFS), or XUV/X-ray coherence tomography (XCT). So far, either large-scale facilities or technologically challenging systems providing only limited photon flux in a single shot dominate the suitable sources. Here, we present a soft, broad-band (1.5 nm - 10.7 nm) soft X-ray source. The source is based on the interaction of very intense laser pulses with a target formed by a cluster mixture. A photon yield of 2.4×10^{14} photons/pulse into 4π (full space) was achieved with a medium containing Xe clusters of moderate-size mixed with a substantial amount of extremely large ones. It is shown that such a cluster mixture enhances the photon yield in the soft X-ray range by roughly one order of magnitude. The size of the resulting source is not beneficial (≤500 µm but this deficit is compensated by a specific spectral structure of its emission fulfilling the specific needs of the spectroscopic (broad spectrum and high signal dynamics) and metrological applications (broad and smoothed spectrum enabling a sub-nanometer resolution limit for XCT).

1. Introduction

Sources emitting photons in the soft X-ray range constitute the essential tools for applications ranging from biology to material science [1] and, more specifically, these tools facilitate extending our knowledge of atomic physics in the gas phase, soft x-ray scattering, magnetic spectroscopy, high-resolution photoelectron spectroscopy, surface chemistry or spectromicroscopy. Typically,

#477726 https://doi.org/10.1364/OE.477726
Journal © 2022 Received 12 Oct 2022; revised 15 Nov 2022; accepted 21 Nov 2022; published 15 Dec 2022

Optics EXPRESS

narrow bandwidth and high brilliance radiation from synchrotron beamlines is applied in so-called user experiments. Easy tunability leading to the wavelength scanning regime is the most used operational property but access to these facilities is still considered limited.

The wavelength range termed as "water window," positioned between 2.3 nm (533 eV) and 4.4 nm (284 eV) is determined by the absorption edges of oxygen and carbon and is particularly interesting for high-contrast studies of biological samples. For spectroscopic applications such as the near edge x-ray absorption fine structure (NEXAFS) or extended X-ray absorption fine structure (EXAFS) focused on the electronic structure of molecules and materials, the beamlines equipped with the spectrometers of very high resolving power are the working horses of the community [2]. These methods require spectral widths of the applied radiation in the range of 30 eV (NEXAFS) and 300 eV (EXAFS). On the other hand, the newly invented and extensively developed XUV/soft X-ray coherence tomography (XCT) [3,4] is a technique demanding broad-band soft X-ray radiation. In this technique, the total reflectivity of layered samples is measured and later processed with an algorithm based on the Fourier transform to provide the structure of the buried reflecting interfaces with a nanometer resolution [5,6]. XCT has been demonstrated in the extreme ultraviolet (XUV) and soft X-ray range by sweeping the photon energy of a synchrotron photon source [5] and by using high harmonics generated in an atomic gas [6,7]. Recently, XCT of 2 nm resolution has been realized with a laser-produced plasma source emitting soft X-rays [8]. The spectral range of extreme ultraviolet (XUV) is especially interesting because the silicon semiconductor nanostructures have a transmission window between 30 and 99 eV. However, many applications demand photons from a broader spectral range, including soft X-rays (100−1000 eV) due to typically very short XUV absorption lengths (tens of nanometers) for most of the elements. The soft X-rays can penetrate many solid samples characterized by the absorption lengths approaching even one micrometer so that NEXAFS/EXAFS and XCT can work with acceptable signal dynamics (high signal-to-noise ratio SNR). Both applications require a high photon flux and highly sensitive and efficient spectrometers [9,10] so that the spectroscopic measurements can be obtained within a reasonably short exposure time.

With the development of compact high-power lasers working at a very high repetition rate [11], secondary photon sources in the soft X-ray range based on high harmonic generation in gases have extensively progressed. With modern high-repetition laser systems operating in the mid-infrared range (MIR), soft X-ray quasi-continua in the "water window" with up to 10^8 photons per second have been demonstrated by applying advanced techniques of the high harmonic generation [12–15]. The advantage of high harmonic sources is the ultra-short pulse duration enabling pump-probe experiments with a temporal resolution even in the range of attoseconds, accompanied by beam divergence lower than that of the driving laser. A disadvantage of the harmonic sources is an adverse scaling rule for single-atom yield $\sim \lambda^{-6.5}$ [14].

Another way of generating soft x-ray radiation exploits the emission from laser-produced plasmas [1]. Dense gas targets [16] and liquid droplets [17,18] were irradiated with the J-class lasers with nanosecond pulse duration to generate suitable plasma. These laser-plasma sources were successfully applied e.g. in compact x-ray microscopy [16–18]. Such sources are typically characterized by a high yield, e.g. 5×10^{11} photons/(sr·pulse) in a single line at 3.37 nm [17] or equivalently a high brightness of 10^{12} photons/(s · sr · μm^2) [18]. In contrast to microscopy, the applications such as NEXAFS or XCT need laser-plasma sources with very broad and smooth spectra. Therefore, the strategy for designing a broadband soft X-ray source relies on merging multiple emission lines to form a spectrally quasi-continuous emission. This strategy applying control over the broadening mechanisms requires ions of higher atomic number, for example, krypton or xenon, and of high density. Alternatively, mixtures of elements, for example, molecular gases, can also be used to obtain more emission lines. In addition, hot plasmas produce higher charge states, which can further broaden the emission lines [19] and shorten the emitted wavelength.

Optics EXPRESS

In this paper, we present a broad-band soft X-ray source emitting radiation in the wavelength range of 1.5 nm to 10.7 nm including the "water window". The source based on the interaction of an intense femtosecond laser pulse with a dense cluster target shows a quasi-continuous spectrum in the specified spectral range and a photon yield of $\simeq 10^{14}$ photons/pulse into full space (4π sr). Based on the theoretical approach it is shown that the demonstrated source is very well suited for such applications as NEXAFS or especially XCT if combined with high resolution spectrometry. The benefits discussed in this work originate from a specific mixture of xenon clusters containing some amount of exceptionally large ones with an average diameter noticeably exceeding the irradiation wavelength [20]. The soft X-ray radiation emitted from such a source confirms its suitability for the mentioned applications. This is reflected in the spectral structure, high conversion efficiency of the irradiation energy into the SXR spectral range including the "water window" as well as the size of the source. An idea of how to improve such a source is also briefly discussed.

2. Experimental setup

A Ti:Sapphire CPA laser system (JETI 40 at the Friedrich-Schiller University in Jena, Germany) operating at a wavelength of 795 nm was used as the laser driver. The laser energy of $\simeq$700 mJ was focused by an f/3 off-axis parabola (OAP) (focal length f = 76.2 mm) and delivered to the target by 40 fs pulses. The laser pulses interact with the target created by a streaming mixture of xenon clusters confined within an external thin stream of helium [20]. A sketch of the experimental arrangement is shown in Fig. 1. For the sake of presenting experimental results we applied the coordinate system with axis z along the beam axis and two transverse directions x, y were selected according to the principles.

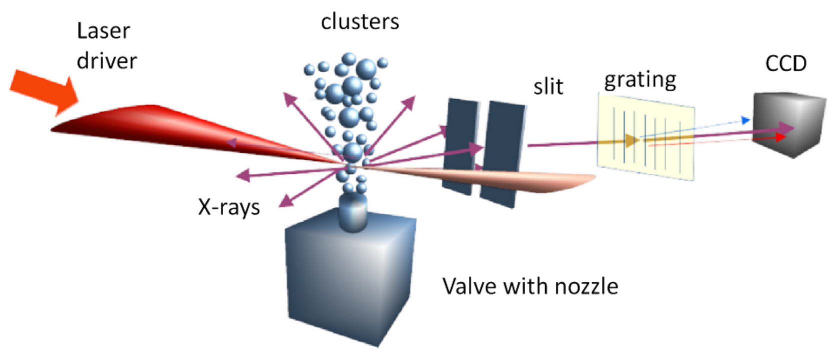

Fig. 1. Sketch of the experimental setup. The outer stream of helium confining the clusters within a limited solid angle is not shown.

2.1. *Target irradiation*

The applied focusing optics resulted in a focal spot area of 3.1×10^{-7} cm^2 (FWHM), and this gave a peak intensity of $\leq 1 \times 10^{19}$ W/cm^2, under the assumption of 40% of the total energy encircled in the focal spot. The temporal pulse profile is an important parameter for the laser-plasma interaction as it determines the dynamics of the ionization and heating processes [21]. The contrast of the irradiating pulse defined as $C(t) = I_{bckgnd}(t) / I_{max}$ (see Fig. 2) was $\leq 10^{-8}$ due to a level of the radiation background originating from the amplified spontaneous emission (ASE), but it was locally worsened by the pre-pulse located $\simeq$ 30 ps in front of the main heating femtosecond pulse, as shown in Fig. 2. The main laser pulse faces different interaction conditions with the clustered matter depending on the background level and its length τ_{bckgnd} in relation to the cluster expansion time τ_{expans} [22]. Typical values of our experimental irradiation conditions and the

Optics EXPRESS

target parameters allowed an estimate of the expansion time to be ~70 - 100 ps for the clusters of a radius of 1.2 µm. This value precludes an efficient contribution of the resonance effect to the total absorption. It is also worth noting that an increase in the cluster size generally lengthens the duration of the short-wavelength emission.

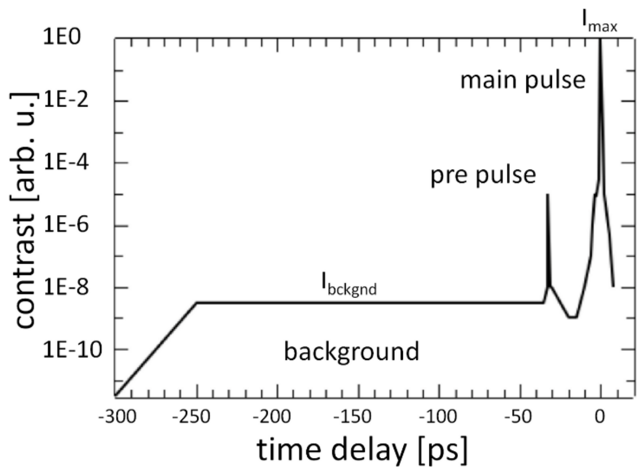

Fig. 2. The temporal profile of the irradiating laser pulse measured with a 3rd-order optical cross-correlator. The waveform is an interpolation created on the basis of those registered in the previous experiments to show the main laser pulse features on the right time scale.

The measurement of the laser pulse shape with a 3rd-order cross-correlator showed that the main part of the background of a length of 200-300 ps (including the pre-pulse) started to increase noticeably 10 ps before the main pulse peak (see Fig. 2). A rough estimate gave a value of 30 J/cm^2 for the incident fluence and ≃10 µJ for the upper limit of the incident background energy. This amount of energy has determined the behavior of the clusters before the arrival of the main, intense laser pulse.

2.2. Cluster target

The mixture of clusters exploited as the target was produced in a stream of working gas (Xe here) injected into a hollow outer stream of an auxiliary gas (He); both were ejected from a double-nozzle gas puff developed at IOE MUT. The detailed target design and the reason for the appearance of extremely large clusters were explained in [20,21]. The design allowed for enhancing not only the working gas density outside the nozzle but also that of the clusters. The interplay of the gaseous streams ejected from the double-nozzle created, when correctly synchronized, a sort of cylindrical nozzle of smoothly varying divergence filled up by the working gas. We performed a delay scan in the range of +/- 300 µs from the optimal laser-target delays. The optimal delays were chosen for maximizing the output signal. Only in that scan range, there was any output emission from our source. The nozzle together with the gas reservoir was thermoelectrically cooled by the Peltier effect down to 245 K. The X-ray yield was maximized at the backing pressures of 4 bar for Xe and 3 bar for He. In the presented case, the average atomic density in the stream approached a value of 8×10^{18} cm^{-3}.

3. Results and discussion

3.1. Laser-cluster interaction

The pioneer works by Ditmire, et al. [23,24] initiated a vigorous pursuit of the phenomena accompanying the interaction between clusters and high-intensity laser radiation and the physical

Optics EXPRESS

scenarios of the processes are well established [23–27]. A cluster benefits from its very high density markedly increasing energy coupling to the matter. Unfortunately, a low average density of the clustered medium is usually the major problem. This deficit was at least partly removed in our arrangement due to the constant pressure exerted by the external gas stream. The pressure of the expanding auxiliary outer gas (He) stream enforced the elimination of the free space surplus by shifting the clusters towards the nozzle axis and for this reason, we termed the "tube" of the external gas the "soft nozzle".

Very large (giant) clusters were less investigated in the past due to the difficulties in forming them even if remarkable attention was paid to droplets of size characterized by a few tens of micrometers [28,29]. Such big objects interact with radiation in a very complex way and after ionization the further path depends on the relation between the cluster size and the duration of the laser pulse [30,31].

Taking into account such an effect, the diversity of the clusters, obtained from our setup, having radii from tens of nanometers to above 1 µm can be considered a unique medium. The number of the available atoms in a single largest Xe cluster (~10^{10}–10^{11} atoms/molecules) is exceptionally large [20]. As a consequence, the laser-matter interaction should result in a broad spectrum of the emitted radiation typical for solid-like targets. Under the available irradiation conditions characterized by a very short laser pulse (30–40 fs) and lack of a plasma mirror (limited pulse contrast), the size of the clusters together with the background radiation became the decisive factors in determining the absorption process and the conversion of the deposited energy into the short-wavelength radiation. The heating process is initiated by optical field ionization [31] followed by a fast collisional absorption [32,33]. Collisions are also the dominant factor in the excitation of the atomic levels involved in emission and this makes it a long-lived process. The latter competes with the re-absorption process. This time scale becomes more significant with an increase in the cluster size due to the accompanying increase in the emission duration.

The laser energy deposition in the gas has to be discussed in relation to the dynamics of the plasma generated in the clustered medium. Taking into account the undetermined expansion scale caused by the pulse background, the main ultra-short laser pulse can meet a partially rarefied medium. The larger clusters will expand slower. Moreover, the quite popular model of spherical expansion [23] is actually no more adequate due to the size of the clusters and the asymmetry enforced by the relation of the cluster size to the laser wavelength [34]. While the interaction starts with tunnel ionization, one can expect a remarkable contribution of the inverse bremsstrahlung (IB) already during the laser pulse due to the very high density of the cluster material. This contribution enables approaching electron energy exceeding 1 keV despite a very short driving laser pulse [32,33]. Any attempt at a detailed analysis of the giant cluster expansion requires separate advanced modeling, and this aspect is out of the paper's scope. Nevertheless, the main features, such as smoothness and expansion scale of the source are easily visible in the temporally integrated images of the source, where the lateral size changes (along the shorter axis of the plasma plume) are induced only by the hydrodynamic effects and are hardly influenced by ionization and the moving breakdown.

3.2. Emission from clusters heated by an intense femtosecond laser pulse

The emission characteristics of the giant cluster target, when irradiated by very intense laser pulses, determined its suitability for applications.

3.2.1. Photon yield

The emission spectrum of the cluster target was recorded for both the cooled and uncooled targets. Each presented spectrum was recorded by averaging over 50 soft X-ray (SXR) pulses, and then it was repeated 3 times under the same nominal irradiation and target conditions. The acquisition geometry is shown in Fig.1(a). The spectrally resolved signal was registered with a transmission grating (2000 l/mm) spectrometer equipped with a 50 µm wide entrance slit. The source's longitudinal axis (the laser propagation axis) created an angle of 45° with the observation direction. The target containing, among others, the giant Xe clusters emitted in a single pulse within the spectral range between 2 nm and 5 nm a number of photons equal to 1.9×10^{13} ph/sr with pre-cooling the gas reservoir and 1.8×10^{12} ph/sr without that. It was found that the conversion efficiency of the laser energy into this soft X-ray isotropic emission from the pre-cooled xenon was about 2×10^{-3} at the applied driving laser intensity. Here, it is worth stressing that the emitted spectrum was significantly broader than that taken in the estimates, and its width exceeded 10 nm (equivalent to $\Delta E \geq 1$ keV), as is seen in Fig. 3.

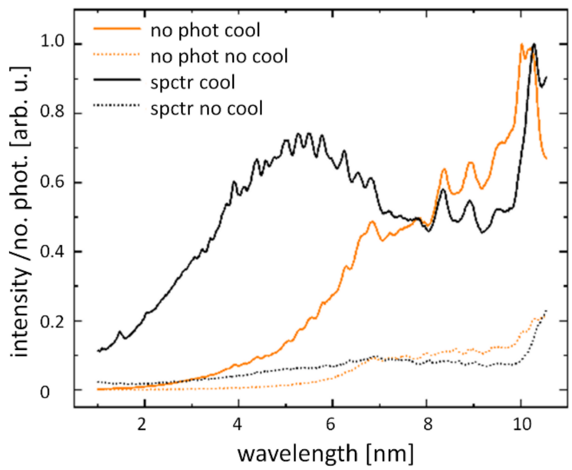

Fig. 3. The spectral intensity distribution (*spctr*) of the xenon emission and the emitted photon numbers (*no. phot.*) for two different temperatures of the reservoir gas: 293 K (denoted as *ncool*) and 245 K (*cool*) transmitted by 0.5-µm Ti filter between source and CCD.

Thus, using the pre-cooled gas resulted in an increase in the number of emitted photons by a factor of 10 for Xe in the spectral range under consideration. This enhancement can be even stronger in the energy domain as the photon number increase is realized mainly by the short-wavelength (more energetic) photons. This is visible in Fig. 3, where a noticeable level of the signal was registered already at a wavelength slightly above 1.0 nm, and this clearly demonstrates that cooling the gas reservoir leads to a significant extension of the emitted spectrum towards shorter wavelengths (more energetic photons). The full spectral range of the recorded emission was roughly between 1 nm (1.2 keV) and 10.7 nm (≃0.115 keV) and it was limited by the detection system. In reality, the low-energy cut-off was even below 0.1 keV. The broad bandwidth definitely predestines the source for spectroscopic applications.

3.2.2. Source size

The irradiation conditions were selected mainly to reveal the tendency in the target performance. The time-integrated dimensions of the short-wavelength source were estimated by applying a pinhole camera with a pinhole diameter of 0.1 mm and a magnification of M = 3.78. The magnification resulted from the source-pinhole and pinhole-camera distances equal to 185 mm and 700 mm, respectively. The image of the source with the real (corrected) dimension values is shown in Fig. 4.

Importantly, we have deliberately modified the dynamics scales of the presentation to stress the difference between the sources in the two considered cases, i.e. the un-cooled gas (Fig.4(a)) and the pre-cooled gas (Fig.4(b)). Many component images were acquired at a single-shot regime

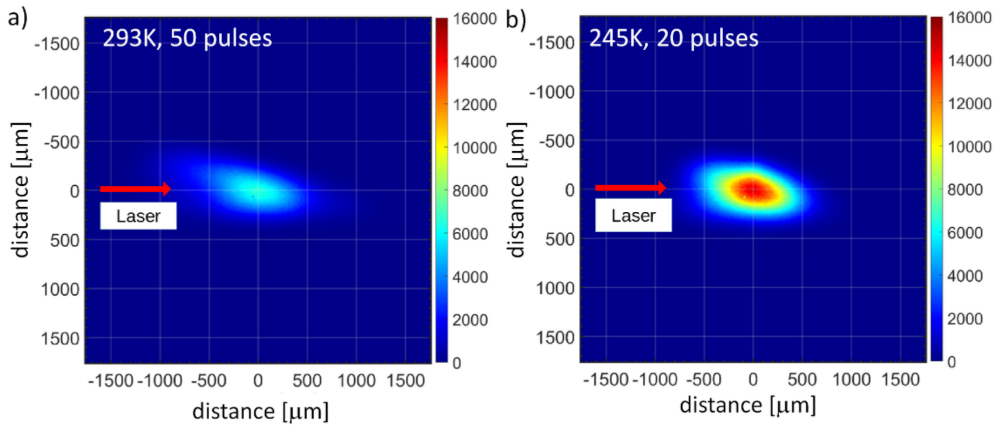

Fig. 4. Contour image of the source's 2D intensity distribution recorded at the emitted short wavelengths when a) the working xenon gas was not cooled, and b) Xe was pre-cooled to a temperature of 245 K. Note that the color bars corresponding to intensity level are equal in both cases to stress the difference in the emission strength while the dynamics of the signal is still artificially reduced by integrating 50 pulses for the panel a) and 20 pulses for the panel b); the red arrows show the incidence direction of the laser beam. Note also that the axes description is recalculated to give the real source dimensions.

at the irradiation conditions optimizing the output. The image of the source – SXR emission from the un-cooled target was integrated over 50 SXR pulses (images), while the emission from the pre-cooled target was integrated over only 20 SXR pulses. Without these means, the signal from the un-cooled target would not be visible at the same dynamics scale. The shape of the source is slightly asymmetric and lacks a clear plasma filament due to, in our opinion, a very intense ionization process. This can be explained by the effects of plasma shielding and the moving breakdown [35]. The dimensions of the fully expanded sources were recorded with a pinhole camera in place of the spectrometer in the experimental set-up presented in Fig. 1. The arrangement included suitable filters (here 500 nm-thick Ti filter was used). The filter transmits moderately the radiation between 1 nm and ~8 nm wavelength.

The source created in the clustered (cooled) Xe performed in a reasonable way. The precooled gas gave the source axial dimension of 481 ± 3 μm and 262 ± 1 μm in the radial direction with the radiant energy of 6×10^{-6} J/sr in a single shot. The corresponding parameters for the gas without pre-cooling were 578 ± 4 μm and 262 ± 1 μm, respectively, with energy of 1.1×10^{-6} J/sr. There are two noteworthy features of the source driven by the intense irradiation of the cluster mixture. Cooling gives always a smaller but more productive emitter. Some contraction of the interaction volume after the clustering process caused by the outer gas stream and more intense ionization in the case of the pre-cooled gas seems to be responsible for that. The energetic yield increased 6 times for the Xe target; the changes introduced by the spectral range and transmission of the filter were taken into account. Here, it should also be stressed that the relatively large pinhole (100 μm in diameter when the estimated optimum diameter was ≃35 μm) contributed to a noticeable uncertainty (overestimate) in the size of the recorded source image (σ_{im}) and required corrections. The calculated errors caused by the blur and diffraction effects were clearly dominated by the former and were taken into account in the corrected source size based on geometrical optics. The absolute value of the blur size was equal to $\sigma_{\mathrm{blur}} = 0.138$ mm, and the diffraction contribution (σ_{diff}) was negligible (~10^{-4} mm). These factors contributed about 29% to the imaged size of the Xe source along the x-axis. The standard formula (1):

$$\sigma_{source} = (\sigma_{im}^2 - \sigma_{blur}^2 - \sigma_{diff}^2)^{1/2}/M \tag{1}$$

was used to estimate the real source sizes (σ_{source}) quoted earlier. For the sake of completeness, it is worth noting that the full lengths of the Rayleigh zone were different in the $x - z$ and $y - z$ planes and were equal to 126 µm and 269 µm, respectively.

The results prove that optimized interaction conditions should further improve the performance of the source and also the evidence of the progress in the targetry development (production of the cluster mixture). The latter could open new ways for progress in the performances of short-wavelength sources as well as laser particle acceleration and neutron generation.

The parameters of a focused beam are important for the transverse resolution of an XCT system. Contrary to the axial resolution, the transverse resolution is not directly related to the optical source. This parameter is determined by the focusing optics combined with the properties of the optical beam that illuminates the sample and can be thought of as the minimum spot size to which an optical beam can be focused. Hence, both the emitted wavelength and the source size come under consideration. While the short wavelength is in favor of this type of resolution, the noticeable transverse dimensions of the source can put some constraints on the achievable focal spot. The transverse resolution of a simple optical system is determined by the expression $\lambda/(2\cdot NA)$ combining the influence of the source wavelength (λ) and collecting power of the optical system related to the source. A high value of numerical aperture (NA) improves the resolution but at the same time limits the depth of field. In practice, this puts a constraint on the possible changes of NA and, as a consequence, limits the source size in a system of reduced radiation collecting power. It is obvious that the spectroscopic experiments require small sources and if necessary one applies slits. This results in photon flux losses.

3.2.3. Spectral modulation

The problem of spectral modulations has already been identified in the standard optical coherence tomography (OCT) schemes and as a consequence, carefully analyzed (see e.g. [36]). The general conclusion was that the spectrum has to be smooth, broad and in the best case, it should possess the Gaussian profile. These properties are generally beneficial for many metrology-related applications and X-ray absorption spectroscopy. The reason for that is obvious when one considers the inverse Fourier transform of the signal reflected from a sample. The inverse transform of the spectral power density (spectral distribution of intensity) of the recorded signal delivers, according to the Wiener-Khintchine theorem, an auto-correlation function (ACF) containing the encoded sample's spatial structure along the normal to the sample surface.

The ACF is directly related to the mutual coherence function (MCF) of the irradiating radiation, and the latter is crucial for the work of the OCT/XCT systems as the radiation coherence length constitutes the main factor determining the resolution of the longitudinal imaging. i.e. along the axis parallel to the normal of the sample surface. A very narrow MCF (and the same is valid for ACF) is required for achieving a very high level of depth's resolution according to the formula derived from the Fourier uncertainty relation for the Gaussian spectral shape [36]

$$\Delta z_{FWHM} = \frac{2\ln 2}{\pi} \cdot \frac{\lambda^2}{\Delta\lambda_{FWHM}} \tag{2}$$

For this reason, coherence of the source contributes to the resolution limit of the system. On the other hand, the inverse Fourier transform (FT^{-1}) of the source power spectrum $S_{source}(\nu)$ gives ACF equal to MCF, frequently denoted as $\Gamma(\tau)$, where τ is for the temporal delay, and ν is the frequency (spectral domain). Thus, MCF becomes the complex depth's point spread function (PSF) modified by or convoluted with the structure of the backscattering profile. Conversion of the source's spectrum to the spatial frequency domain (k) shifts the result of the inverse transform to space in the longitudinal direction (z) [37] and the measured reflected signal can be described

Optics EXPRESS

as

$$I_{SR}(z) = 2\mathrm{Re}\{CSR(z)\} = 2\mathrm{Re}\{S_{source}(z) * h(z)\} \tag{3}$$

where the reflected signal is given by CSR(z) - the cross-spectral power density, h(z) denotes the backscattering profile and * is the convolution operator. The sample model in a form of a stack of Fresnel-reflecting interfaces associates amplitude reflectivities r(z) with the backscattering profile h(z). Thus, the source's ACF can be treated as a form of ideal or ultimate point-spread function (PSF) of the system, i.e. the common image quality metrics, and this has to be as narrow as possible. It is obvious that the source spectral structure will contribute to the effective PSF taking into account also the optical system as well as the longitudinal imaging quality considered as the axial (or depth) resolution level. For the reasons explained earlier, the possibilities of coherence function shaping are very limited and the role of the spectral structure of the source becomes even more important in the case of short-wavelengths. Two different spectra emitted by two laser-plasma X-ray sources (LPXSs) are compared in Fig.5a and Fig.5b.

The spectrum plotted in Fig. 5(a) illustrates a typical spectrum of a dense Xe gas applied frequently in the XCT and spectroscopy experiments up to date, while Fig. 5(b) demonstrates the spectral power density recorded with the new cluster target under investigation. The plots presented in Fig. 5(c) are the corresponding results of the inverse Fourier transform. The visible huge difference in the width of both ACFs confirms the necessity of the source spectrum smoothing. While LPXS based on the standard dense gas target is characterized by ACF having a width (FWHM) of 7.4 nm, the mixture of clusters offers 1.3×10^{-2} nm. Thus, the plots in Fig. 5 illustrate also indirectly the consequences of spectrum modulation for the Γ(z) function.

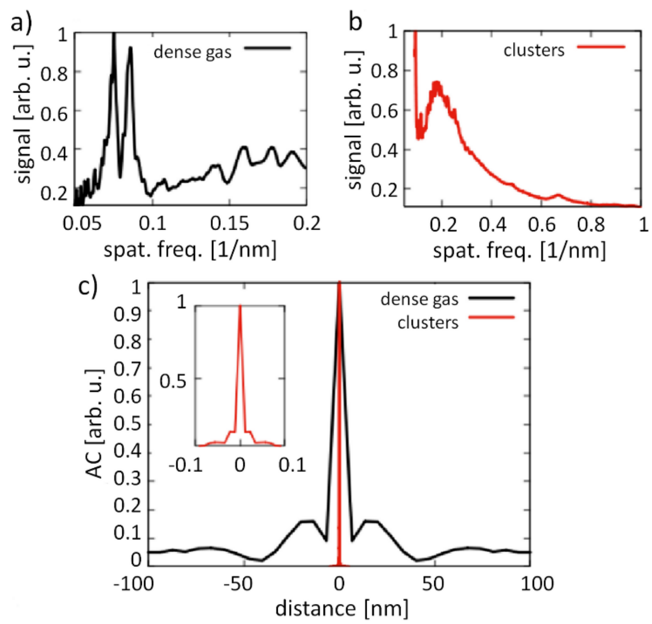

Fig. 5. a) The spectral power density (intensity spectrum) vs. spatial frequency of the xenon emission from plasma generated in a high-density gas ejected from the double-stream nozzle; b) The spectral power density (intensity spectrum) vs. spatial frequency of the xenon emission from plasma generated in the clusters mixture; c) Autocorrelation functions (ACFs) extracted from both intensity spectra (a) and b)) with the inset presenting the ACF of the signal from clusters on a much finer scale.

The degradation of the smooth spectral shape of the source is the cause of the sidelobes in the autocorrelation plot, which, as discussed earlier, leads to an image consisting of multiple

Optics EXPRESS

staggered copies of the desired image. Here, the reference source can be helpful in many aspects, but it cannot improve resolution. These staggered copies of the sample appear as echoes of the highly reflecting interfaces in the OCT/XCT image. The biggest challenge in the design of a suitable source is to combine a large bandwidth with a smooth spectrum shape.

The claim that a Gaussian power spectrum is preferential in OCT/XCT systems does not seem to be an indispensable condition as Fig. 5 clearly demonstrates that even a strongly distorted Gaussian spectrum (if Gaussian at all) still leads to a very narrow ACF.

4. Conclusions

While the laser technology in the spectral ranges of visible (VIS) and near-infrared (NIR) radiation offers many standard techniques facilitating control over the emitted spectrum, the short-wavelength sources based on laser plasma have no such possibilities. As a consequence, only the interaction conditions and the target formation allow the influence on the spectral content of the short-wavelength output at a reasonable expense.

The presented results prove that a mixture of clusters containing among others very large objects ejected from a cooled double-nozzle gas puff facilitates overcoming many drawbacks in using a gas target. It was shown that such a mixture irradiated by an intense laser beam offers very efficient spectral broadening mechanisms leading to a very broad (the spectral bandwidth of $\simeq$1 keV) and relatively smooth spectrum. Such a spectral output is favored in the applications such as X-ray coherence tomography and edge-oriented X-ray absorption spectroscopy. It fulfills the basic requirements crucial for application as a radiation source in these techniques. The photon flux is high, and the power spectrum is not only broad but also sufficiently smooth. The quality of the spectrum features has been confirmed by the estimates of the source ACF. The latter, determined by the inverse Fourier transform of the spectral power density shape, is significantly narrower than that of the typical X-ray sources utilizing dense gas targets. It gives an absolutely new quality. We think that the outer He gas stream efficiently hinders the Xe cluster stream from expanding. As a result, the average cluster concentration increases. On the other hand, the same source delivers a very high photon flux ensuring a reasonably high signal-to-noise ratio (SNR), and enables applying it in spectroscopic experiments of NEXAFS or EXAFS. Both techniques demand a high SNR and in the case of EXAFS also an extremely broad and smooth spectrum.

A reasonable transverse resolution in both applications of interest is connected with the source size and here the noticeable dimension of the source itself enforces using focusing optics. While the spectroscopic application eliminates the problem by introducing a slit of a necessary width (at the expense of photon flux), XCT will need focusing optics. For this reason, the source size should be reduced to limit the losses connected with the application of low-NA optics. The opposite requires an effective increase in the collecting power of the focusing optical system.

Funding. Narodowe Centrum Nauki (2020/39/I/ST7/03194); European Union's Horizon 2020 Laserlab-Europe (871124); internal MUT grant UGB (23-782/2020); Thüringer Aufbaubank (2015FGR0094, 2018FGR0080); Deutsche Forschungsgemeinschaft (PA 730/5, PA 730/9-1); Helmholtz Institute Jena.

Acknowledgments. We gratefully acknowledge the user support of Falk Ronneberger and Burgard Beleites with the JETI40 laser. C.R. acknowledges support from the Hessian Ministry for Science and the Arts (HMWK) through the LOEWE Research Cluster Nuclear Photonics. F. W. is part of the Max Planck School of Photonics supported by BMBF, Max Planck Society, and Fraunhofer Society.

Disclosures. The authors declare that they have no known competing financial interests or personal relationships that could have appeared to influence the work reported in this paper.

Data availability. Data underlying the results presented in this paper are not publicly available at this time but may be obtained from the authors upon reasonable request.

Optics EXPRESS

References

1. D. Attwood and A. Sakdinawat, "X-Rays and Extreme Ultraviolet Radiation," *Principles and Applications*, 2nd ed. (Cambridge University Press, 2017).
2. J. Stohr, *NEXAFS Spectroscopy*, 2nd ed. (Springer, 1996).
3. S. Fuchs, A. Blinne, C. Rödel, U. Zastrau, V. Hilbert, M. Wunsche, J. Bierbach, E. Frumker, E. Forster, and G.G. Paulus, "Optical coherence tomography using broad-bandwidth XUV and soft X-ray radiation," Appl. Phys. B **106**(4), 789–795 (2012).
4. S. Skruszewicz, S. Fuchs, J. J. Abel, J. Nathanael, J. Reinhard, C. Rödel, F. Wiesner, M. Wünsche, P. Wachulak, A. Bartnik, K. Janulewicz, H. Fiedorowicz, and G. G Paulus, "Coherence tomography with broad bandwidth extreme ultraviolet and soft X-ray radiation," Appl. Phys. B **127**(4), 55 (2021).
5. S. Fuchs, C. Rodel, A. Blinne, U. Zastrau, M. Wunsche, V. Hilbert, L. Glaser, J. Viefhaus, E. Frumker, P. Corkum, E. Forster, and G. G. Paulus, "Nanometer resolution optical coherence tomography using broad bandwidth XUV and soft x-ray radiation," Sci. Rep. **6**(1), 20658 (2016).
6. S. Fuchs, M. Wunsche, J. Nathanael, J. J. Abel, C. Rodel, J. Biedermann, J. Reinhard, U. Hubner, and G. G. Paulus, "Optical coherence tomography with nanoscale axial resolution using a laser-driven high-harmonic source," Optica **4**(8), 903–906 (2017).
7. J. Nathanael, M. Wünsche, S. Fuchs, T. Weber, J. J. Abel, J. Reinhard, F. Wiesner, U. Hübner, S. J. Skruszewicz, G. G. Paulus, and C. Rödel, "Laboratory setup for extreme ultraviolet coherence tomography driven by a high-harmonic source," Rev. Sci. Instrum. **90**(11), 113702 (2019).
8. P. Wachulak, A. Bartnik, and H. Fiedorowicz, "Optical coherence tomography (OCT) with 2 nm axial resolution using a compact laser plasma soft X-ray source," Sci. Rep. **8**(1), 8494 (2018).
9. M. Wunsche, S. Fuchs, S. Aull, J. Nathanael, M. Moller, C. Rodel, and G. G. Paulus, "Quasisupercontinuum source in the extreme ultraviolet using multiple frequency combs from high harmonic generation," Opt. Express **25**(6), 6936–6944 (2017).
10. A. Jonas, H. Stiel, L. Gloggler, D. Dahm, K. Dammer, B. Kanngießer, and I. Mantouvalou, "Towards Poisson noise limited optical pump soft X-ray probe NEXAFS spectroscopy using a laser-produced plasma source," Opt. Express **27**(25), 36524–36537 (2019).
11. C. J. Saraceno, D. Sutter, T. Metzger, and M. Abdou Ahmed, "The amazing progress of high power ultrafast thin-disk lasers," J. Eur. Opt. Soc.-Rapid Publ. **15**(1), 15 (2019).
12. S. M. Teichmann, F. Silva, S. L. Cousin, M. Hemmer, and J. Biegert, "0.5-keV Soft X-ray attosecond continua," Nat. Commun. **7**(1), 11493 (2016).
13. B. Buades, D. Moonshiram, T. P. H. Sidiropoulos, I. León, P. Schmidt, I. Pi, N. Di Palo, S. L. Cousin, A. Picón, F. Koppens, and J. Biegert, "Dispersive soft x-ray absorption fine-structure spectroscopy in graphite with an attosecond pulse," Optica **5**(5), 502–506 (2018).
14. T. Popmintchev, M.-Ch Chen, D. Popmintchev, P. Arpin, S. Brown, S. Alisauskas, G. Andriukaitis, T. Balciunas, O. D. Mücke, A. Pugzlys, A. Baltuska, B. Shim, S. E. Schrauth, A. Gaeta, C. Hernández-García, L. Plaja, A. Becker, A. Jaron-Becker, M. M. Murnane, and H. C. Kapteyn, "Bright Coherent Ultrahigh Harmonics in the keV X-ray Regime from Mid-Infrared Femtosecond Lasers," Science **336**(6086), 1287–1291 (2012).
15. Y. Pertot, C. Schmidt, M. Matthews, A. Chauvet, M. Huppert, V. Svoboda, A. Von Conta, A. Tehlar, D. Baykusheva, J. Wolf, and H. J. Worner, "Time-resolved x-ray absorption spectroscopy with a water window high-harmonic source," Science **355**(6322), 264–267 (2017).
16. P. W. Wachulak, A. Torrisi, A. Bartnik, L. Wegrzynski, T. Fok, and H. Fiedorowicz, "A desk-top extreme ultraviolet microscope based on a compact laser-plasma light source," Appl. Phys. B **123**(1), 25 (2017).
17. L. Rymell and H. M. Hertz, "Droplet target for low-debris laser-plasma soft X-ray generation," Opt. Commun. **103**(1-2), 105–110 (1993).
18. H. Legall, G. Blobel, H. Stiel, W. Sandner, C. Seim, P. Takman, D. H. Martz, M. Selin, U. Vogt, H. M. Hertz, D. Esser, H. Sipma, J. Luttmann, M. Höfer, H. D. Hoffmann, S. Yulin, T. Feigl, S. Rehbein, P. Guttmann, G. Schneider, U. Wiesemann, M. Wirtz, and W. Diete, "Compact x-ray microscope for the water window based on a high brightness laser plasma source," Opt. Express **20**(16), 18362–18369 (2012).
19. Spectral Line Broadening by Plasmas, H. E. Griem, ed. in *Series Pure and Applied Physics* 39, 1–410 (1974), Elsevier.
20. L . Wegrzynski, T. Fok, M. Szczurek, A. Bartnik, P. Wachulak, K. A. Janulewicz, and C. M. Kim, "An Abundance of Extremely Large Clusters as a Target for Intense Laser-Matter Interaction," *J. Clust. Sci.* (2022).
21. D. Rupp, "*Ionization and plasma dynamics of single large xenon clusters in superintense XUV pulses*," (Springer Theses, Springer International Publishing Switzerland, 2016); ISBN 978-3-319-28647-1.
22. I. Yu. Skobelev, A. Ya. Faenov, A. I. Magunov, T. A. Pikuz, A. S. Boldarev, V. A. Gasilov, J. Abdallach Jr, G. C. Junkel-Vives, T. Auguste, P. d'Oliveira, S. Hulin, P. Monot, F. Blasco, F. Dorchies, T. Caillaud, C. Bonte, C. Stenz, F. Salin, and B. Yu. Sharkov, "On the interaction of femtosecond laser pulses with cluster targets," J. Exp. Theor. Phys. **94**(1), 73–83 (2002).
23. T. Ditmire, T. Donnelly, A.M. Rubenchik, R. W. Falcone, and M.D. Perry, "Interaction of intense laser pulses with atomic clusters," Phys. Rev. A **53**(5), 3379–3402 (1996).
24. T. Ditmire, "Atomic clusters in ultrahigh intensity light fields," Contemp. Phys. **38**(5), 315–328 (1997).
25. B. M. Smirnov, "Processes in plasma and gases involving clusters," Phys.-Usp. **40**(11), 1117–1147 (1997).

Optics EXPRESS

26. J. Zweiback, T. Ditmire, A. M. Rubenchik, A. Komashko, and M. D. Perry, "Experimental Observation of Resonance Effects in Intensely Irradiated Atomic Clusters," Lawrence Livermore National Laboratory Report UCRL-JC-129764, (1998).
27. F. Dorchies, F. Blasco, C. Bonte, T. Caillaud, C. Fourment, and O. Peyrusse, "Observation of Subpicosecond X-Ray Emission from Laser-Cluster Interaction," Phys. Rev. Lett. **100**(20), 205002 (2008).
28. E. Parra, I. Alexeev, J. Fan, K. Y. Kim, S. J. McNaught, and H. M. Milchberg, "X-ray and extreme ultraviolet emission induced by variable pulse-width irradiation of Ar and Kr clusters and droplets," Technical Digest. Summaries of papers presented at the *Conference on Lasers and Electro-Optics. Postconference Technical Digest (IEEE Cat. No.01CH37170)* (2001), pp. 21–22.
29. S. J. McNaught, J. Fan, E. Parra, and H. M. Milchberg, "A pump–probe investigation of laser droplet plasma dynamics," Appl. Phys. Lett. **79**(25), 4100–4102 (2001).
30. T. Ditmire, T. Donnelly, R. W. Falcone, and M. D. Perry, "Strong X-Ray Emission from High-Temperature Plasmas Produced by Intense Irradiation of Clusters," Phys. Rev. Lett. **75**(17), 3122–3125 (1995).
31. L. Ramunno, T. Brabec, and V. Krainov, *Intense Laser Interaction with Noble Gas Clusters, in Strong Field Physics*, T. Brabec, ed. (Springer Science & Business Media LLC, 2008).
32. W. J. Blyth, S. G. Preston, A. A. Offenberger, M. H. Key, J. S. Wark, Z. Najmudin, A. Modena, A. Djaoui, and A. E. Dangor, "Plasma Temperature in Optical Field Ionization of Gases by Intense Ultrashort Pulses of Ultraviolet Radiation," Phys. Rev. Lett. **74**(4), 554–557 (1995).
33. K. A. Janulewicz, M. Grout, and G. J. Pert, "Electron residual energy of optical-field-ionized plasmas driven by subpicosecond laser pulses," J. Phys. B: At. Mol. Opt. Phys. **29**(4), 901–914 (1996).
34. H. M. Milchberg, S. J. McNaught, and E. Parra, "Plasma hydrodynamics of the intense laser-cluster interaction," Phys. Rev. E **64**(5), 056402 (2001).
35. F. Docchio, P. Regondi, M. R. C. Capon, and J. Mellerio, "Study of the temporal and spatial dynamics of plasmas induced in liquids by nanosecond Nd:YAG laser pulses. Analysis of the plasma starting times," Appl. Opt. **27**(17), 3661–3668 (1988).
36. A. F. Fercher, W. Drexler, C. K. Hitzenberger, and T. Lasser, "Optical coherence tomography - principles and applications," Rep. Prog. Phys. **66**(2), 239–303 (2003).
37. T. Fuji, M. Miyata, S. Kawato, T. Hattori, and H. Nakatsuka, "Linear propagation of light investigated with a white-light Michelson interferometer," J. Opt. Soc. Am. B **14**(5), 1074–1078 (1997).